Contents lists available at ScienceDirect

Colloids and Surfaces A: Physicochemical and Engineering Aspects

journal homepage: www.elsevier.com

# Fine structure of gold nanoparticles stabilized by buthyldithiol: Species identified by Mössbauer spectroscopy

E. Kuzmann,[a, b, *] E. Csapó,[c, *] S. Stichleutner,[d] V.K. Garg,[b] A.C. de Oliveira,[b] S.W. da Silva,[b] L.H. Sing,[b] S.S. Pati,[b] E.M. Guimaraes,[b] A. Lengyel,[a] I. Dékány,[c] K. Lázár [d, *]

[a] *Institute of Chemistry, Eötvös Loránd University, Pázmány Péter sétány 1/A, Budapest, H-1117, Hungary*
[b] *Institute of Physics, University of Brasília, 70919-970 Brasília DF, Brazil*
[c] *MTA-SZTE Supramolecular and Nanostructured Materials Research Group, Department of Medical Chemistry, University of Szeged, Dóm tér 8, Szeged, H-6720, Hungary*
[d] *Centre for Energy Research, MTA, Konkoly Thege út 29-33, Budapest, H-1121, Hungary*

ARTICLE INFO

*Article history:*
Received 11 March 2016
Received in revised form 26 May 2016
Accepted 27 May 2016
Available online xxx

*Keywords:*
Gold nanocluster
Au NPs
$^{197}$Au Mössbauer spectroscopy
Structural identification

ABSTRACT

Stabilized gold nanoparticles (Au NPs) were prepared with 4:2.6 Au to buthyldithiol stoichiometry using modified Brust synthesis. The size of the particles falls into the 1.3–4 nm range in which the molecular cluster – metallic particle transition takes place. Stabilized particles were characterized by transmission electron microscopy (TEM/HRTEM). Moreover, numerous spectroscopic techniques like UV–vis, infrared (FTIR), X-ray diffraction (XRD), Raman, photoacoustic and Mössbauer spectroscopies were also used for detailed structural identification of the functionalized Au NPs. The presence of Au—S bonds was proven by FTIR and Raman spectra. It was found that the distribution of covering thiol layer is uneven, therefore the presence of uncovered surface gold atoms can be assumed at the applied stoichiometry. In good coincidence, four types of gold species could be identified in the corresponding Mössbauer spectrum. They can be attributed to metallic gold in the core, to bare gold in the surface layer, to surface gold atoms attached to thiol, and finally, to gold atoms pulled out from the particle, located in S—Au—S bridges.



## 1. Introduction

Gold nanoparticles (Au NPs) have attracted attention since their first preparation as stabilized sols by Michael Faraday in 1857. Their studies have been enhanced in the last 30–40 years since new fields for applications have been opened recently [1]. Au NPs can be synthesized in a wide size range starting from the assembly of few atoms to stabilized particles with several hundred nanometer size. Stabilization of particles by protecting them with an insulating layer is essential otherwise they easily aggregate. In the low size range there are certain *x* values for $Au_x$ clusters at which their stabilization is preferred (25, 38, 55, 144, *etc.*) [2–5]. Transition from these large molecular complexes (exhibiting separate valence bands) to metallic particles is around at $Au_{55}$, *i.e.* at *ca.* 1.4 nm particle diameter where onset of formation of collective bands can be observed [6]. An important proof of the metallic character is the presence of the characteristic plasmon excitation in the UV–vis spectra at *ca.* $\lambda = 520$ nm which can be observed on particles with diameters exceeding 2–3 nm [7,8]. The 1.4–4 nm size region is specific from another structural point of view, too. Namely, the fcc structure is not prevailing in the Au NPs, instead, multiple twinned particles (MTPs) are composed from aggregation of decahedral, icosahedral and fcc morphologies as XRD and HRTEM studies revealed [9]. Further, the disorder may induce strains in MTPs, up to 4% decrease in the nearest neighbour distance can even be deduced [10].

One of the most rapidly developing fields for applications of Au NPs is their utilization in therapeutics [11]. Small particles with diameters below 2 nm exhibit intense photoluminescence [8,12,13], *e.g.* cytotoxic singlet oxygen can be generated on them by using appropriate photosensitisers [14]. On larger particles, instead of photoluminescence, plasmonic excitation is utilized [15]. As applications, heat can be generated on the particles, selected drug molecules can be released, or they can be used as tracer particles for imaging methods [16–18].

The Au NPs should be stabilized by covering them with a protecting layer. In most cases the particles are prepared by reduction of $Au^{3+}$ salt in a solution with simultaneous covering. Various complex forming ligands (phosphines, amino acids, citrates *etc.*) have been applied for protection so far. Most commonly used is the thiol group (-SH) combined with optional functionalizing groups on the other side of the capping molecules. Interaction of metallic gold with sulphur is the strongest among the optional donor (P, N, O) atoms [19]. The size of Au NPs can be controlled by varying the Au/thiol ratio [20]. Depending on the size various types of gold-sulphur bonds can be formed. Beside the Au—S linear bonds additional monomeric ($Au_{metal}$-SR-Au(I)-SR-$Au_{metal}$) and dimeric ($Au_{metal}$-SR-Au(I)-SR-Au(I)-SR-$Au_{metal}$) "staples" can be formed in large molecular complexes, containing only a few dozens of core gold atoms. These structures are dominant at small thiolate encapped $Au_m$ ($10 < m < 45$) molecular clusters [2,4,21,22] and they can be observed on the sur-

* Corresponding authors at: Centre for Energy Research, MTA, Konkoly Thege út 29-33, Budapest, H-1121, Hungary.
Email addresses: kuzmann@caesar.elte.hu (E. Kuzmann); tidecs2000@yahoo.co.uk (E. Csapó); lazar.karoly@energia.mta.hu (K. Lázár)

http://dx.doi.org/10.1016/j.colsurfa.2016.05.088
0927-7757/

face of larger particles as well [3,23]. On well-developed crystal faces of larger particles thiol molecules may form self-assembled monolayers [24]. In the transient size range (1–3 nm) the encapsulated particles may easily aggregate and sinter, by preserving simultaneously their protecting layers in part [25]. Dithiols exhibit a particular feature, namely their terminal thiol groups on the same molecule may be linked to different Au NPs stabilizing thereby large clusters of them. As a possible application, different vapour sensors can be constructed from these assemblies [26,27].

Besides the commonly used spectroscopic techniques, the $^{197}$Au Mössbauer spectroscopy is also a suitable tool to study gold, but substantially less articles have been published for structural characterization of gold nano-objects using this method. In this technique all the gold atoms (either present inside metallic particles or located in top surface layers) contribute to the detected signals, occasionally in different extents. A particular advantage is that oxidation state of gold can also be derived from spectra [28]. Glutathione encapsulated various $Au_m$ ($10 < m < 45$) molecular clusters have already been characterized by the method, existence of different types of Au—S bonds were revealed [21,29]. Studies were also performed starting from the other, metallic side of the transition region. Namely, neutral metallic particles were obtained by evaporation onto Mylar foil in various diameters (1.5–8 nm) and contributions emerging from core and surface atoms in different extents depending on the size of particles were separated [30].

Study of stabilization of buthyldithiol encapsulated Au NPs is reported in the present work with regard for perspective sensoric applications. Emphasis was also laid on the distinction of various gold-thiol interactions. The size of particles falls into the range of 1.3–3.9 nm, *i.e.* spans over the interval from the molecular cluster to evolving small metallic particle size range. The portion of surface Au atoms compared to entirely core ones is still significant in this range (may extend to *c.a.* 50% of the total amount). Thus, detection of surface Au-S bonds can also be envisaged. Distribution of particle sizes is obtained from TEM images, thicknesses of the protecting layers are estimated from thermogravimetry. The protecting thiolate layers are characterized with optical spectroscopies (FTIR and Raman). Metallic cores are characterized with HRTEM and XRD, while the appearance of characteristic surface plasmon is confirmed by UV–vis. Moreover, Mössbauer spectroscopy is also applied with the presumption that signals originated from the core metallic part and from the surface Au-S bonds can be distinguished.

## 2. Materials and methods

### *2.1. Materials*

The following starting materials were used in the experiments: Gold(III) chloride trihydrate ($HAuCl_4 \times 3H_2O$; ≥99.9% Sigma-Aldrich); tetraoctylammonium bromide (TOABr, 98% Aldrich), 1,4-Butanedithiol ($HS(CH_2)_4SH$, 97%, Aldrich), sodium borohydride ($NaBH_4$, ≥99% Fluka). The toluene and the ethanol solvents were purchased from Molar. All the materials were used without any further purification.

### *2.2. Preparation of buthyldithiol functionalized Au NPs*

Samples were prepared by modified Brust's synthesis [31]. Namely, 8.88 g (16.24 mmol) tetraoctylammonium bromide (TOABr) was dissolved in 300 ml toluene with continuous stirring. Next, after complete dissolution of the TOABr tenside, 16 ml solution of 4 mmol $HAuCl_4 \times 3H_2O$ was added dropwise. The two phases were firmly stirred for 15 min, when Au(III) ions were transferred to the organic phase by TOABr. 300 µl (2.58 mmol) 1,4-buthyldithiol stabilizer was added to the solution afterwards. The reduction of Au(III) to metallic gold was performed by dropwise addition of 100 ml solution of 40 mmol $NaBH_4$. The mixture was stirred for 3 h at ambient temperature. The two phases were separated, 2/3rd of the organic phase was evaporated. The residue, containing the Au NPs was washed with ethanol three times and dried at 50 °C. The obtained product is stable black powder (yield: 70%).

### *2.3. Sample characterization*

The size and the morphology of the nano-objects were studied on images taken with a Technai (200 kV) high resolution transmission electron microscope. The size distribution of the particles was determined by using UTHSCSA Image Tool 2.00 software (University of Texas Health Science Center, San Antonio, TX, USA). HRTEM measurements were performed by a JEM 2100 (JEOL) transmission electron microscope at various magnifications with the accelerating voltage 200 kV. Sample was dispersed in ethanol before fixation of Au NPs on copper grid. X-ray powder diffraction (XRD) measurements were performed at room temperature in the $2\theta = 3–120°$ range by Shimadzu 6000 diffractometer, using $Cu_{K\alpha 1}$ ($\lambda = 0.150562$ nm) radiation. Reflection positions were determined via fitting a Gaussian function. They were reproducible within 0.03°, therefore the uncertainty of the basal spacing was estimated to be ± 0.01 nm. EXRAY code (Eötvös University, Budapest, 1996) was used for the evaluation of diffractograms. Simulation of XRD spectrum and construction of the structural model (see graphical abstract) were carried out by using the CaRine Crystallography 3.1 software [32]. Thermogravimetry measurements were performed by using Mettler Toledo TGA/SDTA851$^e$ in the temperature range of 25–1000 °C using 5 °C/min heat flow profile. UV–vis spectra were recorded on Ocean Optics USB2000 (Ocean Optics Ins., USA) diode array spectrophotometer in the $\lambda = 200–800$ nm range using 1 cm quartz cuvette. The gold powder was redispersed in toluene by ultrasonic agitation. Infrared (IR) spectra were recorded at room temperature using a Fourier Transform Infrared Spectrometer (Bruker VERTEX 70) in transmission mode. Raman spectra were recorded on a DXR Thermo Scientific Dispersive Raman Microscope. The measurements were performed using a 780-nm frequency stabilized single-mode diode laser, at a laser power of 10 mW. For acquisition and evaluation of the spectra, Thermo Scientific OMNIC™ software was used. Photoacoustic (PA) signals resulting from non-radiative de-excitation processes subsequent to excitation by modulated electromagnetic radiation [33] were generated by a 150 W Xe lamp, the light was chopped with frequency of a few Hertz. The variable wavelength was provided by a 0.22 m double monochromator (Spex 1680) with 0.2 nm resolution at 500 nm. Samples were enclosed into a sealed, high-performance, PA cell at atmospheric pressure, coupled to a sensitive microphone [34]. $^{197}$Au Mössbauer spectra were recorded at 4.2 K in a CryoVac cryostat with a built-in Wissel drive and control system using $^{197}$Pt source [35]. Spectra were evaluated by least-square fitting of Lorentzians using the MOSSWINN code [36]. Line widths were constrained to be equal for each component (natural width), the velocity scale is related to $^{197}$Pt.

## 3. Results and discussion

### *3.1. TEM/HRTEM studies*

Size and the morphology of the synthesized thiol-functionalized Au NPs were proven by TEM images. Very small particles were formed in accordance with the expectations of the applied Brust syn-

thesis. Spherical flocculated particles (or so-called large-size clusters) with 30–50 nm diameters can be observed composed from clearly distinguishable Au NPs (Fig. 1A). Distribution of the particle diameters was determined from characteristic TEM images (Fig. 1B). It is seen that the distribution of particle diameters covers the transition interval, spanning from large stabilized molecular clusters (with a core of ~1.5 nm, $Au_{55}$) to larger, but still small size metallic particles. For small particles the fraction of surface layer may be significant. Specifically, for particles with sizes represented on Fig. 1B (top) the portion of the surface monolayer may amount to almost 50% of the total volume. Using a rough simple geometrical approximation considering spherical shape and 0.28 nm diameter for gold atoms, the fractional distributions are shown in Fig. 1B (middle). This distribution is a better approach when results of methods using signals originated from surface atoms or from molecules attached to them are discussed (FTIR, UV–vis). For further comparison, the fractional distribution of the remaining "bulk" metallic component (except the top surface layer) is also shown in the bottom of Fig. 1B. High resolution electron micrographs were also obtained on different Au NPs, one representative image of separate particles is shown in Fig. 2A. The covering layer of buthyldithiol is not evenly distributed around the particles, in one section it is thin, and in another section it is significantly thicker. Further on, it can also be observed that particles with different orientation are glued together with the thiol stabilizing matrix (dark gray patches in between the crystallites in Fig. 2A). Electron diffraction images were also recorded. Rings emerging from (111), (200), (220) and (311) faces of gold crystallites are clearly shown with corresponding lattice distances of 2.355, 2.039 and 1.442 nm, respectively (Fig. 2B).

### 3.2. Thermogravimetry and XRD results

Thermogravimetry is commonly used to obtain a first estimation on the gross thickness of the surface protecting layers. On thiol protected small gold particles (1.5–5 nm range) the weight loss may amount to 15–35 wt% [19,25] depending on the molecular weight of the thiol molecules. The TG curve obtained on our sample is presented in Fig. 3A. Removal of traces of toluene solvent may have taken place in the first 40–120 °C region (23% weight loss). The organic protecting layer is removed in the region of 120–370 °C (15% weight loss). The plateau starting at 400 °C and the modest decrease of weight at higher temperatures is characteristic for metallic gold (62%). Thus, considering the dry sample the thiol: gold sharing is *ca.* 20–80% (by weight). A rough first comparison for contribution of the surface component related to the amount of gold can easily be made by comparing the 20–80% sharing in weight and correcting it with the molecular weight of buthyldithiol and atomic mass of gold atoms. The obtained value for the ratio of the buthyldithiol molecules to the gold atoms is 0.39, which is slightly less than the value extracted from the distribution of particle sizes shown in Fig. 1B (*ca*. 50%). Thus, in the first approximation, a surface coverage of almost one monolayer of thiol can be deduced from the thermogravimetric study.

XRD pattern was also obtained on the thiol stabilized Au NPs (Fig. 3B) in order to determine the individual (primer) particle size of gold colloids. The diffraction peaks at $2\vartheta = 38.23°$, 44.44°, 64.65°,

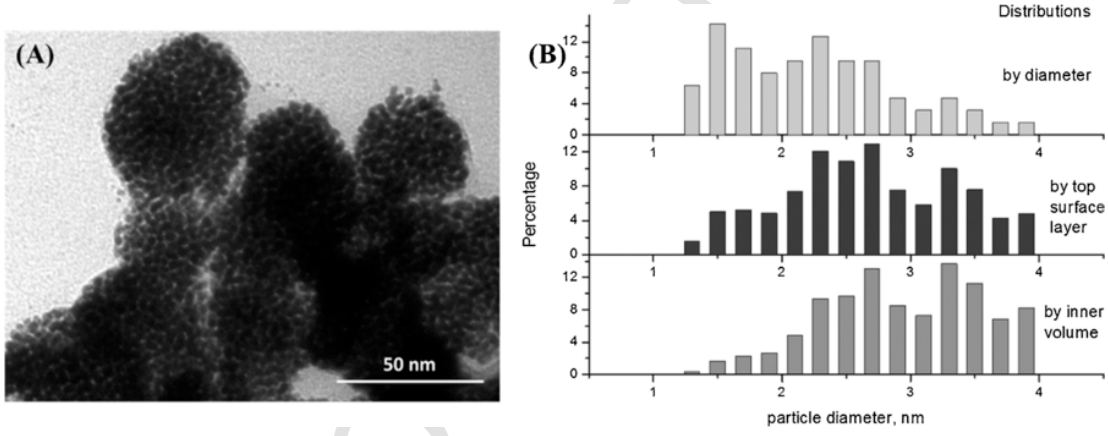


**Fig. 1.** Representative TEM image of the agglomerated Au NPs (A) and the distribution of diameters of Au NPs (top), corresponding estimated volume fractions of monatomic surface layers (middle), and fractions of remaining core volumes (bottom) (B).

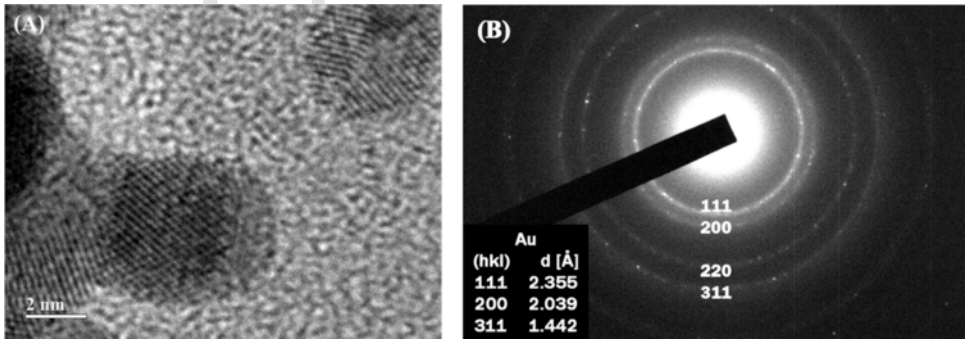


**Fig. 2.** Representative HRTEM image of crystals of Au NPs embedded to the matrix of dark gray patch of buthyldithiol (A) and an electron diffraction image of nanocrystals (B).

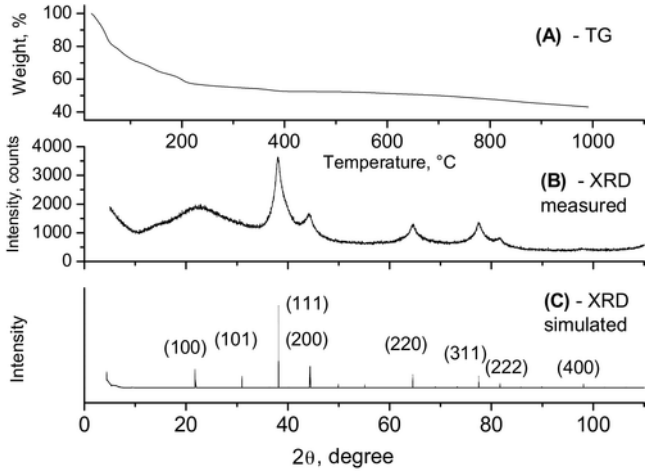


**Fig. 3.** TG curve (A) and XRD pattern (B) of the dithiol stabilized Au NPs, and simulated difractogram of 2 nm fcc gold particles, with dislocations and vacancies (C).

77.67°, 81.83° and 98.28° can be assigned to regular (111), (200), (220), (311), (222) and (400) reflections of fcc gold, respectively, with lattice parameter of a = 0.40740 nm [37] on an amorphous background. Primary size of particles was determined from the broadening of XRD reflections using the Scherrer formula, 2 nm was found for the average diameter [38]. Appearance of the broad peak centered at the 20–22 range can probably be explained with multiple reasons. First, most of it can probably be related to the presence of the intergranular thiol stabilizer [20]. Further, CaRine simulation of 2 nm fcc particles with randomly distributed vacancies and 1/3<422> oriented dislocations results in the appearance of the forbidden (100) and (101) reflections at $2\vartheta = 21.79°$, and 31.01°. The simulated diffractogram is shown in Fig. 3C. As mentioned in the Introduction, multiple twinning may occur in particles of 1.4–4 nm size range and the surface layer can even be amorphous [9,10] thus this approach cannot be excluded either.

### *3.3. UV–vis and photoacoustic spectra*

UV–vis spectra were obtained on a sol (0.01 wt% concentration) prepared by redispergation of the dried particles in toluene by ultrasonic agitation (Fig. 4A) Taking into account the shape of the curve as well as the size of the synthesized nanoparticles the registered spectrum is in good agreement with the experimental results published previously [25,26]. The characteristic plasmonic band appears at around 500 nm, indicating a decrease in particle size [39]. The intensity of this band is small, the smallest particles probably do not contribute to the signal since plasmon excitation does not develop on them [7].

Photoacoustic spectroscopy provides information on molecular species attached to the surface of nanoparticles [34]. Sorption and bonding of some indicator additives may enhance the appearance of signals [40]. Photoacoustic spectrum recorded, in wavelength range between 300 and 1000 nm, on the buthyldithiol stabilized particles is presented in Fig. 4B. In this range one can measure electronic transitions, as gap energy or other electronic excitations or de-excitations. The spectrum can be interpreted in analogy to those obtained under similar experimental conditions on magnetite and Co-ferrite NPs, where three characteristic bands were separated assigned to C (core), S (shell) and L (ligands) [41]. In the present case (Fig. 4B) the first high-intensity band (C band, around 300 nm, with 11.91 au intensity) can be attributed to the core of metallic particles. The peak observed in the spectrum at around 450 nm with 0.48 au intensity is associated

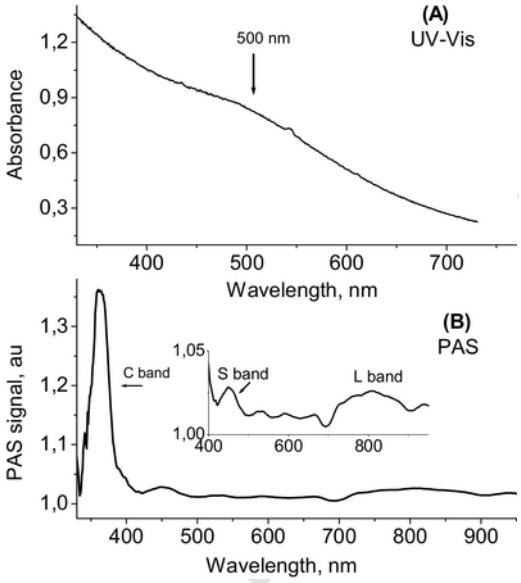


**Fig. 4.** UV–vis (particles redispergated in toluene), (A), and photoacoustic (B) spectra of the Au NPs. (Insert in B for better presentation of S and L bands).

with S band belonging to metallic gold atoms in the shell. The broad L band between 750–850 nm with 2.19 au intensity can be assigned to the presence of the coating thiol layer (Fig. 4B, insert). This can be considered as a superposition of peaks belonging to different bonds related to the ligands. This may indicate the occurrence of different types of sulphur-gold bonds, complementary as being reflected by the $^{197}$Au Mössbauer spectroscopy. The photoacoustic results are in good correspondence with observations obtained with other methods for the covered Au NPs.

### *3.4. FTIR and Raman spectroscopy*

Further details on the composition of the surface coating layer can be revealed from the FTIR spectrum recorded on Au NPs. Numerous other studies report on FTIR spectra of Au NPs with the consent that —S—H bonds disappear upon stabilization, and instead, some Au —S bonds appear in the 5–600 nm region, *e.g.* [19,31,42]. Au—S vibrations appear in small intensity around ~650 $cm^{-1}$ in the spectrum shown in Fig. 5A. Signals of bonds appear at higher frequencies

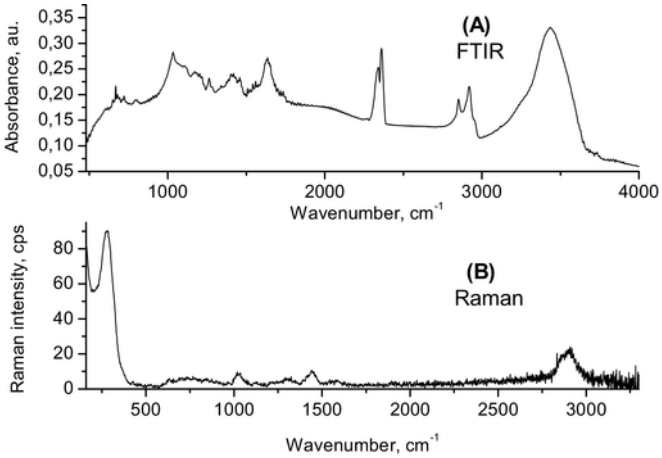


**Fig. 5.** FTIR (A) and Raman (B) spectra of the buthyldithiol protected Au NPs registered in powder form.

for S—C at ~1050, and for S—C—C at ~1600 $cm^{-1}$. Bands of —S—H can still be detected at ~2800 $cm^{-1}$, since —S—H bonds still exist on the opposite, freely dangling end of the buthyldithiol, non- attached to the surface of Au NPs [43]. Raman spectroscopy is also a sensitive tool to study the surface layers. A spectrum was obtained in a wide wavenumber range on Au NPs (Fig. 5B). Appearance of an intense band at 285 $cm^{-1}$ clearly attests for the presence of Au—S bonds in good correspondence with [4]. Other characteristic bands also appear, namely symmetrical skeleton vibration at 1035 $cm^{-1}$, bending and valence vibrations for —$CH_2$— at 1452 and 2926–2853 $cm^{-1}$, respectively. It is worth mentioning that the band for free —SH is missing from the spectrum (it should appear at 2550–2600 $cm^{-1}$). Thus, most of the sulphur atoms in the covering layer is probably linked to gold.

### 3.5. $^{197}$Au Mössbauer spectroscopy

Application of $^{197}$Au Mössbauer spectroscopy was attempted to detect and identify the various gold species. It can be presumed that signals originated from bulk gold in the core of Au NPs and signals from surface gold atoms can be distinguished. The fraction of gold located in the surface monolayer is significant as estimated by simple geometric approach, it amounts to *ca.* 50%, as mentioned earlier (Fig. 1B, middle). Further, the Mössbauer parameters of the surface layer are probably different from those of the bulk core. For instance, a few per cent contraction can be expected on the surface of 1.4–4 nm size particles, and this layer can even be amorphous, as was mentioned earlier [10]. The Mössbauer spectrum of the sample and a proposed decomposition is shown in Fig. 6. Good quality fit could be achieved by a decomposition to four components, the obtained parameters are presented in Table 1. The first singlet component can be assigned to the core of metal particles, since the isomer shift is very close to the nominal value of metallic gold (−1.23 mm/s). This signal is primarily originated from the inner part of larger particles, see Fig. 1B (bottom). The second component can probably be assigned to a surface bare metallic component. Evolution of a surface component with quadrupole splitting in 1.7–3.5 mm/s range in dependence of decrease of particles size is reported in [29]. Analogously, the component with 2.02 mm/s quadrupole doublet may be attributed to these bare surface gold atoms. It is worth noticing that bare surface gold atoms may also exist without Au—S bonds on thiol stabilized surfaces [24]. The third component can be assigned to surface gold

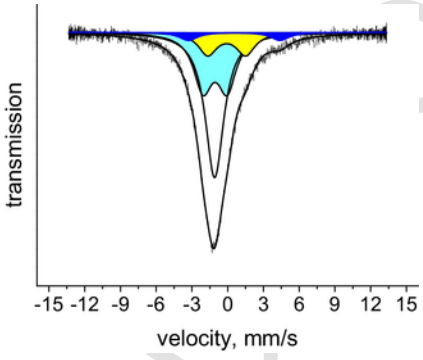


**Fig. 6.** Decomposition of $^{197}$Au Mössbauer spectrum of the butyldithiol stabilized Au NPs recorded at 4.2 K, (central single line: gold, (empty); doublet of bare surface gold: light blue, doublet of Au-S on the surface: yellow, and S-Au(I)-S pulledAu—S on the surface: yellow, and S—Au(I)—S pulled out of the surface: dark blue). (For interpretation of the references to colour in this figure legend, the reader is referred to the web version of this article.)

**Table 1**
Mössbauer data extracted from the decomposition of the spectrum of Fig. 6.

| Component | δ[a] | Δ[b] | Rel. Int.[c] |
|---|---|---|---|
| Au metal-core | −1.10 | – | 46 |
| Au metal-surface | −1.06 | 2.02 | 34 |
| Au in Au-S | −0.08 | 3.18 | 14 |
| Au in S-Au-S | 0.55 | 7.70 | 5 |

[a] isomeric shift, mm/s.
[b] quadrupole splitting, mm/s.
[c] relative intensity, %.

atoms linked to sulphur. For comparison, on thiolate protected gold particles of 2 and 4 nm, 3.47 and 3.07 mm/s values are reported for the quadrupole splitting values, respectively [29] in good correspondence with the quadrupole splitting values shown in Table 1. The fourth component can probably be originated from the middle of the mentioned bridging "staples", namely from gold atoms removed from the metallic surface and located in between two sulphurs, in good correspondence with data reported earlier for this S—Au(I)—S component [3,4,21,23,29]. It is worth noticing that the fraction of the surface components extracted from the relative intensity values shown in Table 1 is 53%. This coincides well with the value obtained from the rough estimation for gold atoms in the top monolayer of spherical particles (~50%). However, this correspondence is probably only occasional, the realistic conditions are more complex. For instance, the probability of Mössbauer effect strongly decreases with the particle size [30], thus the simple geometric approach cannot be used directly for interpretation of relative intensities in Mössbauer spectra of 1.3–4 nm particles.

### 3.6. Stabilization of Au NPs and extent of dithiol coverage

For the fraction of gold atoms located on the surface layer of particles *ca.* 50% is obtained from the rough simple geometric estimation based on distribution of particle diameters shown in Fig. 1B. Another simple approach based on the thermogravimetric analysis results in a similar fraction. This latter estimation is based on the presumption that the surface of the particles is covered with a monolayer of dithiol molecules. Au: dithiol stoichiometric ratio 4:2.6 was used for preparation of stabilized Au NPs. It is a slight excess if both terminal —SH-s of the dithiol are linked to gold. Considering one-arm anchoring and taking into account the *ca.* 50% extent of surface located gold atoms again the same slight excess to 1:1 Au:S ratio can be presumed on the surface. HRTEM images show, however, an uneven coverage and a significant accumulation of dithiol in between the assembled nanoparticles. Thus, certain fraction of the surface gold atoms may probably remain uncovered, not linked to sulphur. Assignment of components in the Mössbauer spectrum is in good accordance with this interpretation, with the decomposition to four components shown previously.

## 4. Conclusion

Properties of buthyldithiol stabilized 1.3–4.0 nm diameter gold particles have been studied. This size interval spans over the 1.3–4 nm range, from large molecular clusters to small (multiple twinning) metallic nanoparticles. Both features are manifested in the results of applied characterizing methods. The metallic properties are primarily represented in XRD diffractogram and in HRTEM images, and in appearance of evolving plasmonic excitations in UV–vis spectrum. Presence of Au—S bonds have been revealed in FTIR and Ra-

man spectra. Among the applied synthesis conditions (4:2.6 Au:dithiol molecular ratio) and considering the uneven coverage and association of particles a fraction of surface gold atom may remain uncovered. In coincidence, four types of gold species can be distinguished in the corresponding Mössbauer spectrum. The two most dominant ones can be interpreted as metallic gold, in the core of particles, and the other as bare Au located on surface. The third gold species is the surface gold linked to sulphur and the fourth minor component can be attributed to gold linked to the surface through S bridges in the —S—Au(I)—S— staples. The presented results may promote the perspective applications of the buthyldithiol stabilized Au NPs in the future.

**Acknowledgements**

The authors are very thankful for the financial support from the Hungarian Scientific Research Fund (OTKA) K 81863 and K 116323 and CAPES (No A127/2013).

**References**

[1] M.-C. Daniel, D. Astruc, Gold nanoparticles: assembly, supramolecular chemistry, quantum-size-related properties, and applications toward biology, catalysis, and nanotechnology, Chem. Rev. 104 (2004) 293–346.
[2] K. Ikeda, Y. Kobayashi, Y. Negishi, M. Seto, T. Iwasa, K. Nobusada, T. Tsukuda, N. Kojima, Thiolate-induced structural reconstruction of gold clusters probed by $^{197}$Au Mössbauer spectroscopy, J. Am. Chem. Soc. 129 (2007) 7230–7231.
[3] H. Häkinnen, The gold–sulfur interface at the nanoscale, Nat. Chem. 4 (2012) 443–455.
[4] B. Varnholt, P. Oulevey, S. Luber, C. Kumara, A. Dass, T. Buřgi, Structural information on the Au-S interface of thiolate-protected gold clusters: a Raman spectroscopy study, J. Phys. Chem. C 118 (2014) 9604–9611.
[5] H. Qiujan, R. Jin, Controlling nanoparticles with atomic precision: the case of $Au_{144}(SCH_2CH_2Ph)_{60}$, Nano Lett. 9 (2009) 4083–4087.
[6] G. Schmid, B. Schmid, Nanoparticulated gold: syntheses, structures, electronics, and reactivities, Eur. J. Inorg. Chem. (2003) 3081–3098.
[7] M.M. Alvarez, J.T. Khoury, T.G. Schaaff, M.N. Shafigullin, I. Vezmar, R.L. Whetten, Optical absorption spectra of nanocrystal gold molecules, J. Phys. Chem. B 101 (1997) 3706–3712.
[8] S. Eustis, M.A. El-Sayed, Why gold nanoparticles are more precious than pretty gold: noble metal surface plasmon resonance and its enhancement of the radiative and nonradiative properties of nanocrystals of different shapes, Chem. Soc. Rev. 35 (2006) 209–217.
[9] D. Zanchet, B.D. Hall, D. Ugarte, Structure population in thiol-passivated gold nanoparticles, J. Phys. Chem. B. 104 (2000) 11013–11018.
[10] A. Cervellino, C. Giannini, A. Guagliardi, D. Zanchet, Quantitative analysis of gold nanoparticles from synchrotron data by means of least-squares techniques, Eur. Phys. J. B 41 (2004) 485–493.
[11] J. Gao, X. Huang, H. Liu, F. Zan, J. Ren, Colloidal stability of gold nanoparticles modified with thiol compounds: bioconjugation and application in cancer cell imaging, Langmuir 28 (2012) 4464–4471.
[12] J.P. Wilcoxon, J.E. Martin, F. Parsapour, B. Wiedenman, D.F. Kelley, Photoluminescence from nanosize gold clusters, J. Chem. Phys. 108 (1998) 9137–9143.
[13] D. Philip, Synthesis and spectroscipic characterization of gold nanoparticles, Spectrochim. Acta Part A 71 (2008) 80–85.
[14] D.C. Hone, P.I. Walker, R. Ewans-Gowing, S. FitzGerald, A. Beeby, I. Chambrier, M.J. Cook, D.A. Russell, Generation of cytotoxic singlet oxygen via phthalocyanine-stabilized gold nanoparticles, Langmuir 18 (2002) 2985–2987.
[15] V. Hornok, E. Csapó, N. Varga, D. Ungor, D. Sebők, G. Laczkó, I. Dékány, Controlled synthesis and structural characterization of plasmonic and red-emitting gold/lysosyme nanohybride dispersions, Colloid. Polym. Sci. 294 (2016) 49–58.
[16] D. Pissuwan, T. Niidome, M.B. Cortie, The forthcoming applications of gold nanoparticles in drug and gene delivery systems, J. Control. Release 149 (2011) 65–71.
[17] G. Han, P. Ghosh, V.M. Rotello, Functionalized gold nanoparticles for drug delivery, Nanomedicine (Lond.) 2 (2007) 113–123.
[18] A. Agarwal, S.W. Huang, M. O'Donell, K.C. Day, M. Day, N. Kotov, S. Ashkenazi, Targeted gold nanorod contrast agent for prostate cancer detection by photoacoustic imaging, J. Appl. Phys. 102 (2007) 064701.
[19] W. Shi, Y. Sahoo, M.T. Swihart, Gold nanoparticles surface-terminated with bifunctional ligands, Colloids Surf. A: Physicochem. Eng. Asp. 246 (2004) 109–113.
[20] F. Vitale, I. Frattoddi, C. Battochio, E. Piscopiello, L. Tapfer, M.V. Russo, G. Polzonetti, C. Giannini, Mono- and bi-functional arenethiols as surfactants for gold nanoparticles: synthesis and characterization, Nanoscale Res. Lett. 6 (2011) 103.
[21] N. Kojima, Y. Kobayashi, Y. Negishi, M. Seto, T. Tsukuda, Structural evolution of glutathionate-protected gold clusters studied by means of $^{197}$Au Mössbauer spectroscopy, Hyperfine Interact. 217 (2013) 91–98.
[22] I. Dolamic, B. Varnholt, T. Bürgi, Far-infrared spectra of well-defined thiolate protected gold clusters, Phys. Chem. Chem. Phys. 15 (2013) 19561–19565.
[23] P.D. Jadzinsky, G. Calero, C.J. Ackerson, D.A. Bushnell, R.D. Kornberg, Structure of a thiol-monolayer protected gold nanoparticle at 1.1 Å resolution, Science 318 (2007) 430–433.
[24] D. Fischer, A. Curioni, W. Andreoni, Decanethiols on gold: the structure of self-assembled monolayers unraveled with computer simulations, Langmuir 19 (2003) 3567–3571.
[25] B.L. Smith, J.E. Hutchison, Transformations during sintering of small ($D_{core}$ < 2 nm) ligand-stabilized gold nanoparticles: influence of ligand functionality and core size, J. Phys. Chem. C 117 (2013) 25127–25137.
[26] N. Molnár-Vörös, R. Patakfalvi, I. Dékány, Alkylthiol-functionalized gold nanoparticles for sensing organic vapors, Colloids Surf. A: Physicochem. Eng. Asp. 329 (2008) 205–210.
[27] D. Sebők, E. Csapó, N. Ábrahám, I. Dékány, Reflectometric measurement of n-hexane adsorption on ZnO nanohybrid film modified by hydrofobic gold nanoparticles, Appl. Surf. Sci. 333 (2015) 48–53.
[28] R.V. Parish, Gold-197 Mössbauer spectroscopy in the characterization of gold compounds, In: G.J. Long (Ed.), Mössbauer Spectroscopy Applied to Inorganic Chemistry, Vol. I, 1984Plenum, pp. 577–617.
[29] N. Kojima, K. Ikeda, Y. Kobayashi, ·T. Tsukuda, Y. Negishi, G. Harada, ·T Sugawara, M. Seto, Study of the structure and electronic state of thiolate-protected gold clusters by means of $^{197}$Au Mössbauer spectroscopy, Hyperfine Intreract. 207 (2012) 127–131.
[30] L. Stievano, S. Santucci, L. Lozzi, S. Calogero, F.E. Wagner, $^{197}$Au Mössbauer study of gold particles obtained by evaporation of metallic gold on Mylar, J. Non-Cryst. Solids 232-234 (1998) 644–649.
[31] M. Brust, J. Fink, D. Bethell, D.J. Schiffrin, C. Kiely, Synthesis and reactions of functionalised gold nanoparticles, J. Chem. Soc. Chem Commun. (1995) 1655–1656.
[32] http://carine.crystallography.pagespro-orange.fr (accessed 24.05.16).
[33] A. Rosenzwaig, A. Gersho, Photoacoustic effect with solids: theoretical treatment, Science 190 (1975) 556–557.
[34] S.R. Avelino, F.M.L. Oliveira, A.C. Oliveira, P.C. Morais, Use of photoacoustic spectroscopy in the investigation of the dilution process in surface-coated nanoparticles, J. Non-Cryst. Solids 352 (2006) 3692–3698.
[35] T. Belgya, K. Lázár, New in-beam Mössbauer spectroscopy station at the budapest research reactor, Hyperfine Interact. 167 (2006) 875–879.
[36] Z. Klencsár, E. Kuzmann, A. Vértes, User-friendly software for Mössbauer spectrum analysis, J. Radioanal. Nucl. Chem. 210 (1996) 105–118.
[37] JCPDS card: 04-0784.
[38] B. Streszewski, W. Jaworski, K. Pacławski, E. Csapó, I. Dékány, K. Fitzner, Gold nanoparticles formation in the aqueous system of gold(III) chloride complex ions and hydrazine sulfate—kinetic studies, Colloids Surf. A 397 (2012) 63–72.
[39] L.B. Scaffardi, N. Pellegri, O. de Sanctis, J.O. Tocho, Sizing gold nanoparticles by optical extinction spectroscopy, Nanotechnology 16 (2005) 158–163.
[40] B.S. Gutrath, M.F. Beckmann, A. Buchkremer, T. Eckert, J. Timper, A. Leifert, W. Richtering, G. Schmitz, U. Simon, Size-dependent multispectral photoacoustic response of solid and hollow gold nanoparticles, Nanotechnology 23 (2012) 225707.
[41] A.C. Oliveira, A.L. Tronconi, N. Buske, P.C. Morais, Photoacoustic spectroscopy of magnetic fluids, J. Magn. Magn. Mater. 252 (2002) 56–58.
[42] M. Farrag, M. Tschurl, A. Dass, U. Heiz, Infra-red spectroscopy of size selected $Au_{25}$, $Au_{38}$ and $Au_{144}$ ligand protected gold clusters, Phys. Chem. Chem. Phys. 15 (2013) 12539.
[43] N.B. Colthup, L.H. Daly, S.E. Wiberley, Introduction to Infrared and Raman Spectroscopy, Academic Press, 1975.